The vibrational spectrum of $CaCO_3$ aragonite. A combined experimental and quantum-mechanical investigation

Cédric Carteret,[1] Marco De La Pierre,[2] Manuel Dossot,[1]
Fabien Pascale,[3] Alessandro Erba,[2] and Roberto Dovesi[2]

[1]*Laboratoire de Chimie Physique et Microbiologie pour l'Environnement (LCPME), UMR 7564, Université de Lorraine - CNRS, 405 rue de Vandœuvre, 54601 Villers-lès-Nancy, France*

[2]*Dipartimento di Chimica, Università di Torino and NIS -Nanostructured Interfaces and Surfaces - Centre of Excellence, http://www.nis.unito.it, Via P. Giuria 7, 10125 Torino, Italy*

[3]*5Q, rue du Beaujolais 54500 Vandœuvre-lès-Nancy Cedex 05, France*

(Dated: December 6, 2012)

Abstract

The vibrational properties of $CaCO_3$ aragonite have been investigated both theoretically, by using a quantum mechanical approach (all electron Gaussian type basis set and B3LYP HF-DFT hybrid functional, as implemented in the CRYSTAL code) and experimentally, by collecting polarized infrared (IR) reflectance and Raman spectra. The combined use of theory and experiment permits on the one hand to analyze the many subtle features of the measured spectra, on the other hand to evidentiate limits and deficiencies of both approaches. The full set of TO and LO IR active modes, their intensities, the dielectric tensor (in its static and high frequency components) and the optical indices have been determined, as well as the Raman frequencies. Tools such as isotopic substitution and graphical animation of the modes are available, that complement the analysis of the spectrum.

Keywords: IR spectra, Raman spectra, reflectance, polarized, single crystal, ab initio simulation, frequencies, intensities, CRYSTAL code

I. INTRODUCTION

Calcium carbonate nucleates in three crystalline forms: calcite, aragonite and vaterite, with rhombohedral, orthorhombic and hexagonal structure, respectively. Calcite is the most stable thermodynamically, followed by aragonite. The crystallization of calcium carbonate is a widely occurring process in nature (marble and limestone, biominerals, etc.)[1] as well as a relevant operation in industry. Calcium carbonate is one of the main components of the scaling which arises in various drainage situations in the chemical industry, and in circulating water for heating and cooling in living environments[2]. Calcium carbonate is also used as an additive in various industrial fields, e.g. building materials, medicines, food, paper, plastics, printing inks[3]. Although calcite is the most stable $CaCO_3$ phase at Earth surface conditions, aragonite is a very common mineral, of both biological and geological origins. In particular, aragonite is the major constituent of coral reefs, shells, pearls and other biominerals, where it grows preferentially at ambient conditions due to the effect of organic templates [4]. Aragonite occurs in many other environments as deposition of hot, mineral-rich springs, in stalactite and stalagmite cave formations [5].

For these reasons aragonite, along with the other naturally occurring polymorphs, has been the subject of a large number of investigations using a variety of techniques. The infrared (IR) and Raman spectra of aragonite were collected in the past by several investigators, who applied group theory to classify the active modes. Polarized Raman spectra of aragonite were first measured by Couture [6]. This pioneering work was completed by Frech *et al.* [7] who produced accurate Raman polarized spectra and some IR reflectance spectra. More recently the IR and Raman spectra have been used as an analytical tool by chemists and mineralogists to separate the carbonate polymorphs: calcite, aragonite, and vaterite [8–12]. Although the vibrational spectra of aragonite have been previously measured, the assignment of the normal modes is incomplete; moreover, no IR data are available in the far-infrared range, and the dielectric function in the far- and mid-infrared ranges is still unknown. This is probably due both to difficulties in obtaining a well-characterized single crystal of sufficient optical quality and to the absence of accurate references from simulation, two ingredients that constitute novelty elements of the present investigation. The polarized Raman and IR reflectance spectra in the whole spectral range are here obtained from a high quality single crystal whose orientation was determined by X-ray diffraction. Besides that, accurate *ab*

initio simulations are performed, that complement the experimental data and provide an extremely useful support in their processing.

It is in fact well known that, whereas the "final results", namely frequencies and intensities, are directly produced by Raman experiments, their determination from the raw-digitalized IR reflectance spectrum $R^{exp}(\nu)$ is not simple, and implies a best fit procedure. As the fitting parameters are strongly correlated and the χ^2 function to be minimized is characterized by many minima, additional information must be available during the optimization process, to be inserted in the form of constraints. One of the crucial points of this process is the definition of the number and position (on the frequency axis) of oscillators to be used in this non-linear best fit; in other words, a set of quite reasonable initial parameters must be provided. It should be noticed that the number of active modes (provided *a priori* by group theory) might not correspond to the number of modes present in the spectrum, as some of them might be characterized by very low intensity. The presence in the best fit process of a spurious oscillator can introduce additional numerical instability. On the other hand, combinations and resonances might be interpreted as fundamentals, if the theoretical number of modes is looked for persistently.

At this stage, the availability of a simulated spectrum, that can nowadays be easily generated by quantum mechanical codes, can dramatically reduce the risk of erroneous attributions or artefacts. This permits to discriminate among the fundamental peaks characterized by low (often very low) intensity and other features such as combinations, overtones, Fermi resonances and impurities.

The paper is organized as follows: Section II is devoted to the description of the sample. Information on the Raman and IR experimental set up is also provided. Section III describes the way simulation is performed. In Section IV the results from theory and experiment are compared. Section V presents the main conclusions.

II. EXPERIMENTAL DETAILS

A. Sample, orientation, convention

$CaCO_3$ aragonite has an orthorhombic unit cell with parameters[13] $a = 4.9618$, $b = 7.9691$, $c = 5.7429$ Å, four formula units (Z=4), and $Pnma$ space group (D_2^{h16} in Schönflies

notation). The original sample was oriented by X-Ray Diffraction (XRD), cut and polished to reveal the (100), (010), and (001) facets. The final size of the sample is $\sim 5 \times 4 \times 2$ mm^3 along the a, b, c axes, respectively. XRD confirms that our sample is a single $CaCO_3$ aragonite phase with lattice parameters (at room temperature) $a = 4.9633$, $b = 7.9703$, $c = 5.7441$ Å, which are very close to the ones from the literature [13] (see also Table I).
Figure 1 shows the orientation of the CO_3 triangles with respect to the crystallographic axes. The x, y and z Cartesian axes, according to the current laboratory reference, were selected as the a, b and c crystallographic axes, respectively. B_{3u}, B_{2u} and B_{1u} symbols were used for the polarization along a, b and c, respectively.

B. Polarized Infrared Reflectance spectroscopy and best fit

Polarized IR spectra $R^{exp}(\nu)$ were measured at room temperature (295 K) along the three crystallographic directions a, b and c. The selected spectral range was 80-2500 cm^{-1}, with a resolution of 1 to 2 cm^{-1}. A near-normal angle of incidence ($\theta = 10°$) was chosen. The s-polarized geometry was employed, as it has been shown to reduce the contamination from other crystallographic directions [14, 15].
A reconstructed reflectance curve $R^{fit}_{ii}(\nu)$ along the ii direction can be obtained by best fit of $R^{exp}_{ii}(\nu)$, by means of the Fresnel formula[16]:

$$R^{fit}_{ii}(\nu) = \left| \frac{\sqrt{\epsilon_{ii}(\nu) - sin^2(\theta)} - cos(\theta)}{\sqrt{\epsilon_{ii}(\nu) - sin^2(\theta)} + cos(\theta)} \right|^2 , \quad (1)$$

where θ is the incidence angle of the IR beam with respect to the normal to the surface and $\epsilon_{ii}(\nu) = \epsilon_{1,ii}(\nu) + i\epsilon_{2,ii}(\nu)$ is the $ii-th$ component of the complex dielectric function. The maxima of $\epsilon_2(\nu)$ and of Im(-1/$\epsilon(\nu)$) (Loss Function) correspond to the TO and LO frequencies, respectively. Note that, when the symmetry of the system is orthorhombic or higher, $\epsilon(\nu)$ is a diagonal tensor, so that only the xx, yy and zz components are non-null.
The classical Drude-Lorentz model [16] describes the dielectric function as a superposition of damped harmonic oscillators:

$$\epsilon_{ii}(\nu) = \epsilon_{\infty,ii} + \sum_n L_{n,ii}(\nu) , \quad (2)$$

where $\epsilon_{\infty,ii}$ is the high-frequency (electronic) dielectric contribution and the oscillator $L_{n,ii}(\nu)$ is defined as:

$$L_{n,ii}(\nu) = \frac{f_{n,ii}\nu_n^2}{\nu_n^2 - \nu^2 - i\nu\gamma_n} \ . \tag{3}$$

Each oscillator is characterized by three parameters: the frequency ν_n of the TO mode (note: only of the TO mode), its strength along the ii direction $f_{n,ii}$ (related to the plasma frequency $\nu_{p,n}$ through $f_n = \nu_{p,n}^2/\nu_n^2$) and the damping factor γ_n. These quantities can be obtained by best fit, through minimization of the chi-square (χ^2) between $R_{ii}^{fit}(\nu)$ and $R_{ii}^{exp}(\nu)$ over a set of points on which the latter has been digitalized.

An alternative semi-quantum model was also adopted, that was introduced by Berreman and Unterwald[17] and applied for the first time by Gervais and Piriou[18, 19]. It contains four parameters, namely the frequencies ν of both the TO and LO modes and the corresponding damping factors γ:

$$\epsilon_{ii}(\nu) = \epsilon_{\infty,ii} \prod_n \frac{\nu_{LO,n}^2 - \nu^2 - i\nu\gamma_{LO,n}}{\nu_{TO,n}^2 - \nu^2 - i\nu\gamma_{TO,n}} \ . \tag{4}$$

where the n product extends to all the modes corresponding to the ii direction. The $ii-th$ component of the $n-th$ oscillator strength can be calculated by comparison of Equations 2 and 4 in which the damping is neglected [18]:

$$f_{n,ii} = \epsilon_{\infty,ii} \left(\frac{\nu_{LO,n}^2}{\nu_{TO,n}^2} - 1 \right) \prod_{k \neq n} \frac{\nu_{LO,k}^2 - \nu_{TO,n}^2}{\nu_{TO,k}^2 - \nu_{TO,n}^2} \ . \tag{5}$$

This model permits to take into account the asymmetry of the reflectance peaks (that in many cases is quite large).

Best fit procedures against the Drude-Lorentz (DL) and Four-Parameter Semi-Quantum (FPSQ) models were performed with the RefFIT interactive program written by Alexey Kuzmenko [20]. The simulated frequencies and intensities were used as an initial guess for the fits. First, damping factors were determined; then, individual mode parameters were optimized iteratively within a finite window around the simulated data (30 cm^{-1} for frequencies, 30 % for intensities). In the case of modes with very low intensities, this window was reduced by a factor 3 to 4. Finally, a constrained global minimization on all the parameters was performed.

C. Polarized Raman spectroscopy

Raman spectra were collected at 295 K on a Jobin-Yvon T64000 spectrometer coupled to a N_2-cooled CCD detector and an Olympus optical microscope. Samples were excited by an argon-ion laser beam at 514.5 nm using a Spectra Physics Stabilite 2017 laser. The laser beam was focused on the sample via a 16x microscope objective with approximately 20 mW excitation power. Back-scattered Raman spectra were collected in confocal mode with a low numerical aperture objective to avoid optical artifacts; Rayleigh scattering was removed by an edge filter. The Raman spectra were recorded between 90 and 1600 cm^{-1}, with acquisition times of 2 minutes and a spectral resolution of about 1.5 cm^{-1}.
The crystal was deposited at the center of a rotation stage and oriented along either a, or b or c axes. A careful adjustment was made of the rotation stage, to ensure the overlap of the focused laser with the center of the rotation stage. The polarized Raman measurements were performed using a polarizer for both cross and parallel configurations (i.e. with respect to the incident laser polarization vector) and referred for the (100) orientation to as $x(zz)\overline{x}$ and $x(yz)\overline{x}$ respectively, according to Porto's notation[21]. The notation of the spectrum is described by four symbols, two inside parentheses and two outside. The inside symbols are, left to right, the polarizations of the incident and scattered beams, while the letters preceding and following the parentheses indicate the respective propagation directions of the incident and scattered beams.

III. COMPUTATIONAL METHODS

For the present calculations, the CRYSTAL program[22, 23] was used. As in previous works by some of the present authors [24–29] the B3LYP Hamiltonian[30] was employed, that contains a hybrid Hartree–Fock/density–functional exchange–correlation term, and is widely and successfully used in molecular quantum chemistry[31] as well as in solid state calculations, where it has been shown to reproduce vibrational frequencies in general good agreement with experiment.[32–35].
The adopted basis set has already been used in a previous investigation of calcite (BSD in Ref. 36). Oxygen, calcium and carbon are described by $(8s)-(411sp)-(1d1d)$, $(8s)-(6511sp)-(2d1d)$, $(6s)-(311sp)-(1d1d)$, contractions, respectively. Details can be

found at the web page `www.theochem.unito.it/aragonite`, where input and output files are also available.

The computational conditions (tolerances for the truncation of the infinite Coulomb and exchange sums, SCF convergence criteria, grid size for the integration of the DFT exchange and correlation contribution and number of points in the reciprocal space) were set at the same values as in a previous study on calcite[36].

The calculation of vibrational frequencies at the Γ point, ν_n, was performed within the harmonic approximation. Frequencies are obtained by diagonalizing the mass-weighted Hessian matrix W, which is constructed by numerical differentiation of the analytical gradients with respect to the atomic Cartesian coordinates:

$$W_{\alpha i,\beta j}(\Gamma) = \frac{H_{\alpha i,\beta j}}{\sqrt{M_\alpha M_\beta}} \ , \tag{6}$$

where $H_{\alpha i,\beta j}$ is the second derivative of energy (evaluated numerically starting from the analytical gradients), M_α and M_β are the atomic masses; greek and latin indices refer to atoms and atomic Cartesian coordinates, respectively. The calculated (optimized) equilibrium geometry is taken as reference. Once the Hessian matrix is calculated, frequency shifts due to isotopic substitutions can be readily obtained by changing the masses in the above formula, so that isotopic-shift calculations are available at zero computational cost. Details on the calculation of vibrational frequencies can be found in Refs. 24, 35, and 37.

The oscillator strengths f_n were computed for each $n-th$ mode by means of the mass-weighted effective mode Born charge vectors $\vec{Z}_n$ [38, 39]:

$$f_{n,ij} = \frac{1}{4\pi\epsilon_0}\frac{4\pi}{\Omega}\frac{\vec{Z}_{n,i}\vec{Z}_{n,j}}{\nu_n^2} \ , \tag{7}$$

$$\vec{Z}_{n,i} = \sum_{\alpha,j} \mathbf{t}_{n,\alpha j} Z^*_{\alpha,ij} \frac{1}{\sqrt{M_\alpha}} \ , \tag{8}$$

where ϵ_0 is the vacuum dielectric permittivity ($1/4\pi\epsilon_0 = 1$ atomic unit), Ω is the unit cell volume, i and j refer to the Cartesian components, $\mathbf{t}_{n,\alpha j}$ is an element of the eigenvectors matrix T of the mass-weighted Hessian matrix W, that transforms the Cartesian atomic directions into the $n-th$ normal coordinate directions; finally, Z^*_α is the Born effective charge tensor associated with atom α, which is evaluated through a Berry phase approach [40–42].

The ionic components of the static dielectric tensor were evaluated as the sum of the oscillator strengths: $F_{ij} = \sum_n f_{n,ij}$. The electronic high frequency components $\epsilon_{\infty,ij}$ were

calculated through the Coupled-Perturbed KS/HF (Kohn-Sham/Hartree-Fock) scheme [43–47]. Note that ϵ_∞ is almost independent from frequency in the IR range, as electronic transition energies are very large compared to vibrational energies.

Graphical animations of the normal modes are available on the CRYSTAL web site (`www.crystal.unito.it/prtfreq/jmol.html`); they provide a simple and intuitive interpretation of the "nature" of the modes (stretching, bending, rotation, translation, etc).

Manipulation and visualization of structures were dealt with the MOLDRAW program [48, 49] and the JMOL[50] molecular viewer. Molecular drawings were rendered with the Inkscape program [51] using input files prepared with Jmol. Data analysis was performed with the LibreOffice suite [52].

IV. RESULTS AND DISCUSSION

A. Geometry

The structure of the orthorhombic unit cell of aragonite is shown in Figure 1, and the main parameters are reported in Table I. The B3LYP calculation overestimates the experimental cell parameters by 0.9% (a), 0.7% (b) and 2.0% (c) , which is typical for this type of Hamiltonian (see, for example, Ref. 27). Also the distances with a large ionic/dispersion contribution, such as Ca-O (note that the Ca ion is largely polarizable), are slightly overestimated, by about 0.02 Å. Differences reduce by one order of magnitude, to about 0.001 Å, in the case of the strong covalent C-O bond.

B. Frequencies at the Γ point

The orthorhombic cell of aragonite (see Figure 1) contains 4 $CaCO_3$ formula units, for a total of 20 atoms; its 57 vibrational modes can be classified according to the irreducible representations of the mmm point group as follows:

$$\Gamma_{total} = 9A_g \oplus 6A_u \oplus 6B_{1g} \oplus 8B_{1u} \oplus 9B_{2g} \oplus 5B_{2u} \oplus 6B_{3g} \oplus 8B_{3u}.$$

A_g, B_{1g}, B_{2g} and B_{3g} modes are Raman active, B_{1u}, B_{2u} and B_{3u} are IR active, A_u modes are spectroscopically inactive (silent modes). Modes are classified as "internal" and "external" in Table II. The latter (rotations and translations of the CO_3^{--} and Ca^{++} units)

appear below 300 cm^{-1}. The former (24 modes overall) form four well separated bands, that correspond to symmetric stretching (1080-1090 cm^{-1}, usually indicated as ν_1), out-of-plane bending (850-910 cm^{-1}, ν_2), antisymmetric stretching (1440-1580 cm^{-1} , ν_3) and in-plane bending motions (700-720 cm^{-1}, ν_4). Such a classification is confirmed by graphical animation (`www.crystal.unito.it/prtfreq/jmol.html`) and is in agreement with the very old one proposed by White in 1974[53].

C. IR reflectance spectra

Figure 2 shows the results of the best fit performed with the three-parameter Drude-Lorentz (DL) model. Values for frequencies ν and oscillator strengths f obtained from the best fit are given in Table III, where they are compared with the quantum-mechanically simulated data.

The reflectance spectra R_{DL}^{fit} constructed by using Equations 1, 2 and 3 reproduce quite accurately R^{exp}, with the evident exception of the right shoulder of the first broad band along the b axis (see Figure 2(b)). The best fit was repeated with the Four-Parameter Semi-Quantum (FPSQ) model described by Equation 4, looking for a better reproduction of this band. A zoomed view of the range 150-450 cm^{-1} for the b axis is reported in Figure 3, where both R_{FPSQ}^{fit} and R_{DL}^{fit} spectra are superposed to the experimental curve; the fitting parameters for the b axis are reported in Table IV, where the two models are compared. Mode 3, with TO frequency ν_{TO} around 220 cm^{-1}, corresponds to the observed broad band. While ν_{TO} provided by the two models is about the same (the difference is 1.1 cm^{-1} only), the other parameters show relevant differences. f and ν_{LO} differ by as much as 790 (adimensional; all values are multiplied by 10^3) and 17.4 cm^{-1}, respectively. As regards the damping factors, the FPSQ model provides distinct values for TO and LO modes; γ_{TO} is quite close to the (unique) γ value provided by the DL model, 7.3 cm^{-1} compared to 9.0 cm^{-1} (the difference being 1.7 cm^{-1} only). γ_{LO} is however considerably larger ($\Delta\gamma^{FPSQ} = 28.1$ cm^{-1}). All these differences permit the FPSQ model to properly describe the asymmetry in the observed experimental band. For the other modes differences are smaller, and involve only one or two of the fitting parameters. The largest ones refer to mode 1 ($\Delta f = 240$) and mode 5 ($\Delta\nu_{LO} = 14.3$ cm^{-1}, $\Delta f = 52$). The improved agreement between the reconstructed R_{FPSQ}^{fit} spectrum and R^{exp} for the b axis is demonstrated by χ^2_{FPSQ}, that is smaller than χ^2_{DL} by a

factor 9. As a comparison, in the case of a and c axes, when passing from the DL to the FPSQ model, χ^2 improves only by a factor 2: no relevant asymmetric bands exist along these axes, and the reduction is essentially due to the higher number of degrees of freedom in the best fit model.

The observed quite good agreement between R_{DL}^{fit} (or R_{FPSQ}^{fit}) and R^{exp} is obtained thanks to an initial guess for the fitting that uses the calculated *ab initio* frequencies and intensities. Without this help, the best fit would have been much more problematic, as a look to Table III easily confirms. Consider for example the a direction (B_{3u} symmetry). There is a very large peak at 208 cm^{-1} (210 cm^{-1} from the calculation), with oscillator strength equal to 4106 (3920 from the calculation). There are three peaks (ν_{exp} at 183, 259 and 287 cm^{-1}) whose f is from 50 to 100 times smaller than the largest one. Two peaks have f in the order of 2 and 0.1, and finally one peak ($\nu_{calc} = 1469$ cm^{-1}) has null calculated oscillator strength. The identification of peaks 5 and 7 (see zooms in Figures 4(a) and 4(c)), whose f is three to four orders of magnitude smaller than the dominant peak, would have been impossible through the fitting process alone, i.e. without the guidelines provided by simulation. Note that Frech *et al.* (1980)[7] have reported no data in the far infrared range and, by focusing on the high frequency region 650-1600 cm^{-1}, have been able to identify only 7 out of the 10 fundamental IR peaks.

The null calculated intensity of mode 8 (Figure 4(d)) permits to reduce the number of oscillators to 7, and to eliminate from the fitting process three variables that would further increase the correlation among all the parameters. The weak and broad feature in the 1450-1550 cm^{-1} experimental range (see again Figure 4(d)) is likely to be related to the very intense bands appearing along the a and c axes in the same interval: it should be attributed to leakage, and/or non perfect orientation of the sample.

It is worth to underline that peaks 5 and 7 are extremely small features of the spectrum. There are other similar "minor" features that might in principle be taken into account in the fitting process, so that only the comparison with the simulated spectrum permits to select the ones that correspond to fundamental frequencies. A similar "zoom", with almost the same scale as for peaks 5 and 7, is shown in Figure 4(b), to focus on the small peak located by the best fit at 844 cm^{-1}: as in this spectral region there are no calculated fundamental modes, this feature should be attributed to a combination mode, as proposed by White[53] and Donoghue *et al.*[54]. We can generate all the direct products of cou-

ples of fundamental modes that yield a mode with B_{3u} symmetry. The only combination whose frequency is reasonably close to the observed one is 699.8 (B_{2u}) + 151.7 (B_{1g}) = 851.5 cm^{-1}, which is only 8 cm^{-1} higher than the experimental value. Graphical animation (`www.crystal.unito.it/prtfreq/jmol.html`) shows that the former mode is an in-plane bending of a single C-O bond in each CO_3^{--} unit, while the latter mode is an out-of-plane libration of each unit around the axis defined by the same C-O bond.

A similar analysis of the intense and weak peaks of the spectrum might be performed for the b and c axes as well. Note that the lattice bands in the three polarization directions strongly overlap, so that measurements on powder samples would be unlikely to reveal all the details observed in this single crystal study.

The refractive (n) and absorption (k) indices can be obtained as a by-product of the best fit, starting from the complex dielectric function. They are shown in Figure 5 for the three crystallographic directions.

D. IR frequencies and intensities

Let us now compare quantum-mechanically calculated and experimental frequencies and intensities, shown in Table III; the corresponding statistics are reported in Table V.

For TO modes the agreement is excellent for all but two frequencies, with a difference never larger than 10 cm^{-1}. The mean absolute difference $\overline{|\Delta|}$ is as small as 6.3 and 5.2 cm^{-1} for the a and c axes, respectively. It increases to 14.1 cm^{-1} for the b axis, due to two large differences (underestimations) for modes 1 and 3 (-40 and -22 cm^{-1}, respectively). The reason why these two modes are too soft is related to the B3LYP (slight) overestimation of the lattice parameters. In order to quantify the relevance of this effect, calculations were repeated at the experimental lattice parameters (all inner fractional coordinates having been re-optimized). The results for the b axis (Table VI) show a systematic increase of the frequencies between 5 (high frequencies) and 28 (low frequencies) cm^{-1}. Indeed, modes 1 and 3 turn out to be the most sensitive to the volume change, with an increase of 28 and 23 cm^{-1}, respectively. The mean absolute deviation $\overline{|\Delta|}$ with the experiments reduces to 7.5 cm^{-1} (from 14.1 cm^{-1}). A similar behavior at low frequencies has already been identified in the case of a soft Mg mode at 134 cm^{-1} in pyrope garnet [27].

Similar considerations hold for the LO frequencies (reported in Table III, too), the mean

and maximum absolute deviations being very close to the TO ones. In this case, the two frequencies with deviations larger than 10 cm^{-1} in modulus are mode 1 of axis b (again, -33 cm^{-1}) and mode 8 of axis c (+17 cm^{-1}, i.e. only 1%).

As regards the oscillator strengths (Table III, multiplied by 10^3), in general the agreement is excellent. Taking into account that they span 4 orders of magnitude, f^{exp} and f^{calc} are always very close: for values larger than 20, differences do not exceed 30% in all but one case. An overall measure of the quality of f values is given by $F = \sum_n f_n$, that is the ionic contribution to the static dielectric tensor (see Table VII). For the a and c directions F^{exp} and F^{calc} differ by only -4% and +9 %, respectively. In the case of b the difference increases to +70%, as a consequence of the very large oscillator strength of mode 1. If this mode is excluded from the statistics, the difference reduces to +18%. The huge simulated f value for this mode is connected to the underestimation of its frequency. Again, at the experimental cell parameters (Table VI) the agreement of all the oscillator strengths for the b axis improves. In particular, f for mode 1 reduces from 6555 to 3670, which is considerably closer to the experimental value at 2228.

The calculated TO-LO splittings $\delta\nu$ are in good agreement with the experimental TO-LO splittings (Table III). The only two differences larger than 10 cm^{-1} (B_{2u} modes 3 and 5) occur for $\delta\nu$ larger than 100 cm^{-1}, so that the relative difference is smaller than 10%. Large splittings of the transverse and longitudinal components are associated to modes with large oscillator strengths (i.e. large dipole moment variations), and result in broad reflectance bands. This is the case of out-of-phase translations of CO_3^{--} and Ca^{++} units (modes B_{1u} 3, B_{2u} 3, B_{3u} 2) and of CO_3^{--} antisymmetric stretchings (modes B_{1u} 8 and B_{2u} 5).

Finally, let us comment on the values for the optical dielectric tensor ϵ_∞, reported in Table VII. Calculated values for the three axes are 2.181, 2.660 and 2.674, slightly smaller (-6%, -5% and -5%, respectively) than the experimental determinations. This trend is typical for B3LYP calculations (see, for example, Ref. 27).

E. Raman frequencies and spectra

Several aragonite experimental Raman spectra have been reported before the one produced in the present study[6, 7, 9, 55]. In particular, Alía (1997)[55] has collected the unpolarized spectrum of a polycrystalline sample; Frech *et al.* (1980) [7] have performed

polarized Raman measurements over a single crystal, as in this work; both experiments have been carried out at room temperature. Since presently we are unable to provide computed values for the Raman intensities (whose calculation is currently being implemented in the CRYSTAL code), simulation can be used only for predicting the frequencies. However, as the Raman experimental spectra are more directly comparable with simulation and provide directly the frequency of the modes, with no need of fitting through models, the available information from simulation is sufficient to identify most of the modes absent in previous determinations.

All sets of frequencies are listed in Table VIII; the present experimental spectra are shown in Figures 6 and 7. The three experimental determinations are in quite good agreement among them when the common subset of modes is considered: the mean absolute deviations with each other are around only 1 cm^{-1}. Frech *et al.* have identified 23 distinct peaks, while Alía has reported 19 peaks. As for the IR, comparison with simulation permits us to identify more modes than in previous studies, i.e. 27 out of the 30 that are symmetry allowed. The overall agreement between simulated and experimental frequencies is excellent, the mean absolute deviation $\overline{|\Delta|}$ being 6.4 cm^{-1} (Alía), 6.6 cm^{-1} (Frech *et al.*) and 5.8 cm^{-1} (present study). In this latter case, the largest errors are found at low frequencies, namely for mode 25 (-21 cm^{-1}) and mode 10 (-15 cm^{-1}). Both of them are close to 100 cm^{-1}; the explanation for the large underestimation is the same as for mode 1 of the IR spectrum along the b axis (B3LYP overestimation of the lattice parameters). Note also a difference much larger than 10 cm^{-1} for mode 24 around 1500 cm^{-1} (18 cm^{-1}, i.e. 1.1%).

Let us now focus on the features that would have been hard to identify without the help of simulation (see Figures 6 and 7 as a reference). The main difficulty is the complete identification of the sets of modes for each single symmetry; the reason is that there are several modes with different symmetry but very close frequency. Frech *et al.* have missed four modes with respect to the present study: peaks 13 and 15 (B_{1g} symmetry), peak 23 (B_{2g} symmetry) and peak 26 (B_{3g} symmetry); they are highlighted by arrows in Figure 6. In all these cases, Frech *et al.* have found the peaks in the spectra, but have assumed they were leakages of very intense peaks from other symmetries (peaks 4, 9, 8 and 16, respectively).

The study by Alía has been complicated by the fact that he has performed unpolarized Raman measurements on a polycrystalline sample, so that no symmetry assignment has been possible. In addition to the four modes missed by Frech *et al.*, Alía has not identified four

additional modes (see again the arrows in Figures 6 and 7). Two of them have been covered by leakage: peak 3 (A_g symmetry, superposed to peak 27) and peak 14 (B_{1g}, hidden by peak 6). Moreover, the two B_{2g} peaks 22 and 24 have not been found at all, most probably due to their low intensity.

There are three modes that appear in our simulation but do not have any experimental counterpart; they lie at 199 (B_{1g}), 279 (B_{2g}) and 1415 (B_{3g}) cm^{-1}. If we inspect the experimental curves in the corresponding regions, even by expanding the intensity scale (not shown) we are unable to identify any spectral feature. This suggests that these three modes must be characterized by very low, or even null, intensity.

Finally, it is worth commenting on the A_g peak at 1060 cm^{-1} (Figure 7), which does not match any of the computed Raman frequencies, thus is not a fundamental mode. Upon isotopic substitution analysis, simulation suggests to attribute it to a ^{18}O isotope satellite mode of the very intense peak at 1086 cm^{-1}. The simulated isotopic shift is 20 cm^{-1}, in good agreement with the experimental one (26 cm^{-1}); moreover, this is the only simulated mode that shows a significant shift upon ^{18}O isotopic substitution. Graphical animation (`www.crystal.unito.it/prtfreq/jmol.html`) shows that the mode at 1086 cm^{-1} is the symmetric C-O stretching in the CO_3^{--} units. Indeed, when a ^{16}O atom is substituted with the ^{18}O isotope, animation shows that CO_3^{--} units with only "regular" ^{16}O atoms still stretch at 1086 cm^{-1}, while units bearing the ^{18}O isotope decouple from the others and stretch at 1060 cm^{-1}. Further evidence comes from the relative intensities of the two peaks. The experimental ratio is about 1/200, which implies a 0.5 % abundance of CO_3^{--} units bearing a ^{18}O atom, and thus a 0.17 % abundance of this isotope in the sample. This value is extremely close to ^{18}O natural abundance, i.e. 0.2 %.

V. CONCLUSIONS

We have presented a combined experimental and computational investigation of the Infrared (IR) reflectance and Raman spectra of $CaCO_3$ aragonite. The analysis has been carried out in a very integrated way, so that strengths of the two approaches are exploited synergically.

Fitted and experimental IR spectra are in excellent agreement. For one IR band of B_{2u} symmetry, the three-parameter Drude-Lorentz model used for interpreting the experimental

spectrum is in part unsatisfactory. When the more sophisticated Four-Parameter Semi-Quantum model (taking into account peak asymmetry by describing TO and LO modes separately) is adopted, the agreement for this peak improves substantially, whereas it remains unaltered for the other peaks. Spectral features, that would be hardly recognized as peaks due to low intensity, are clearly identified thanks to comparison with simulation. Overall, 20 fundamental modes were assigned, out of the theoretical 21. On the other hand a clearly visible peak at 844 cm^{-1} in the B_{3u} spectrum is missing from the list of computed fundamental IR modes, so that it is characterized as a combination mode.

Computed and experimental (fitted) IR frequencies and intensities are in very good agreement, the mean absolute deviations being 7.8 cm^{-1} and 335, respectively. A large fraction of these differences is due to modes at 105 and 220 cm^{-1} in the B_{2u} spectrum. In this case the discrepancy is attributed to the computational method, in particular to the well known lattice overestimation typical for the B3LYP Hamiltonian.

Raman frequencies are in excellent agreement, too (mean absolute deviation 5.8 cm^{-1}). In this case, the comparison with simulation permits to identify a certain number of peaks, that were not recognized in previous studies due to superposition with other peaks or low intensity; 27 (out of 30) Raman modes were characterized. An experimental feature at 1060 cm^{-1} in the A_g spectrum is absent in the calculation; it has been identified as a ^{18}O isotope mode of the very intense peak at 1086 cm^{-1}.

For both IR and Raman spectra the availability of computed frequencies is crucial for a complete identification of the modes in the spectra, and for their classification.

VI. ACKNOWLEDGEMENTS

The authors acknowledge Compagnia di San Paolo for financial support (Progetti di Ricerca di Ateneo-Compagnia di San Paolo-2011-Linea 1A, progetto ORTO11RRT5). Computer support from the CINECA supercomputing centre is kindly aknowledged. CC would like to thank F. Brehat and B. Wyncke for fruitful discussions and continuous support.

FIGURES

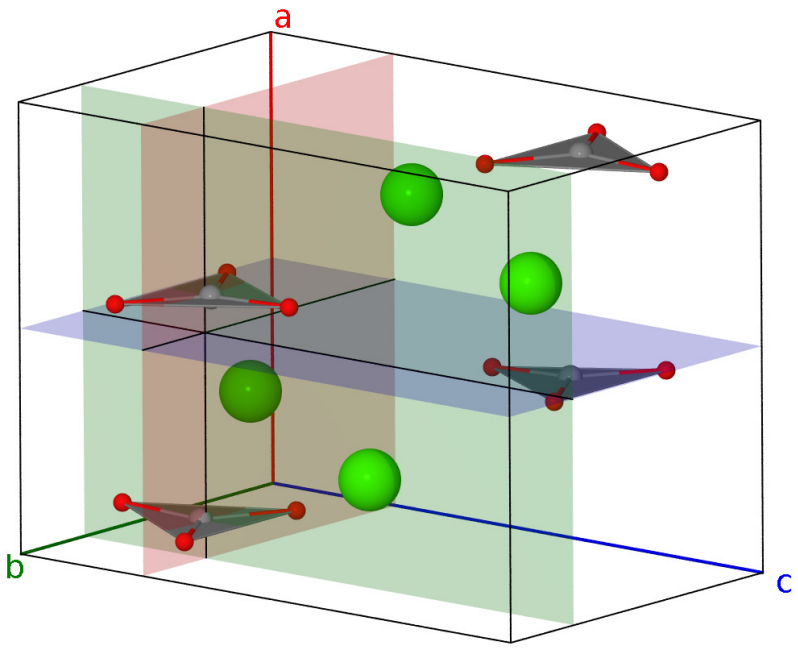

FIG. 1. Orthorhombic unit cell of aragonite (*Pnma* space group), containing four CO_3^{--} units and four Ca^{++} ions. The Cartesian frame is chosen so that x, y and z axes coincide with a, b and c, respectively. Symmetry planes are drawn as well.

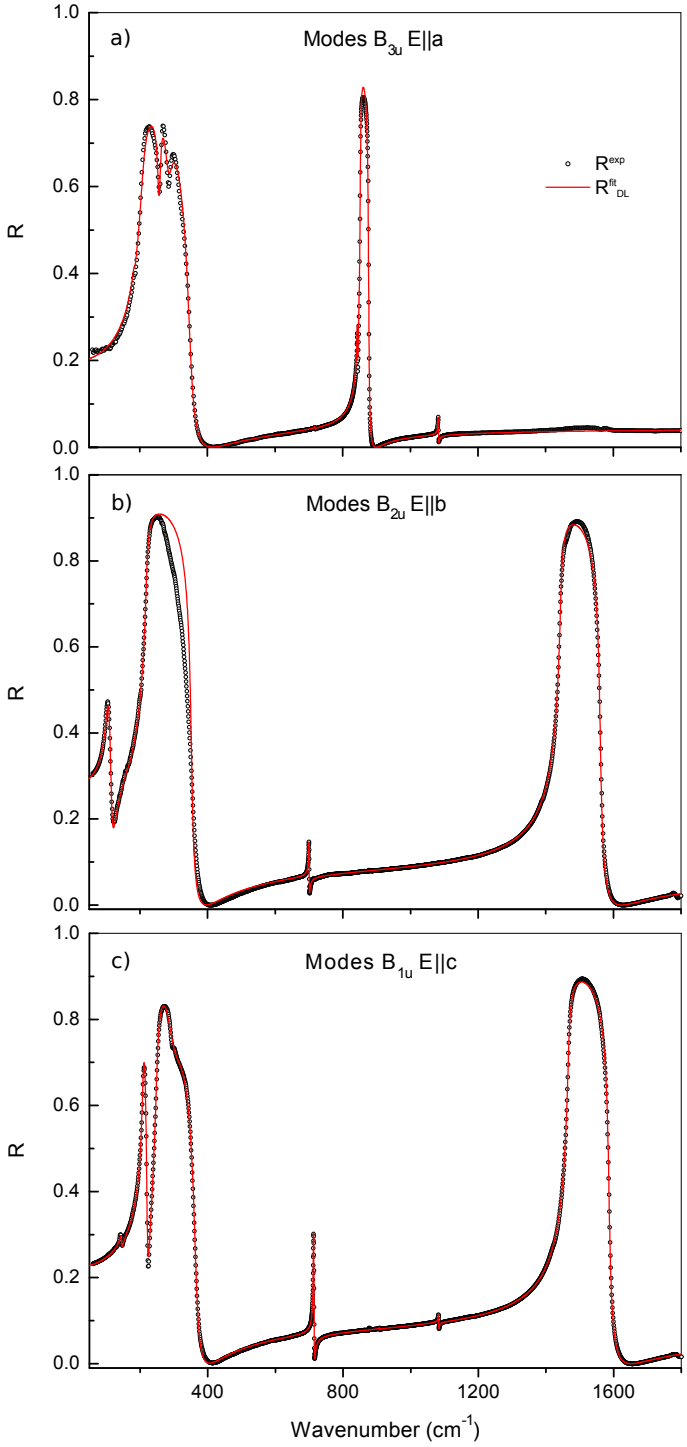

FIG. 2. IR reflectance spectra along a, b and c axes of aragonite: experimental data (points) versus fitted curve (solid line). The fitting is performed based on the three-parameter Drude-Lorentz model, by taking the quantum-mechanically computed frequencies and oscillator strengths as starting values.

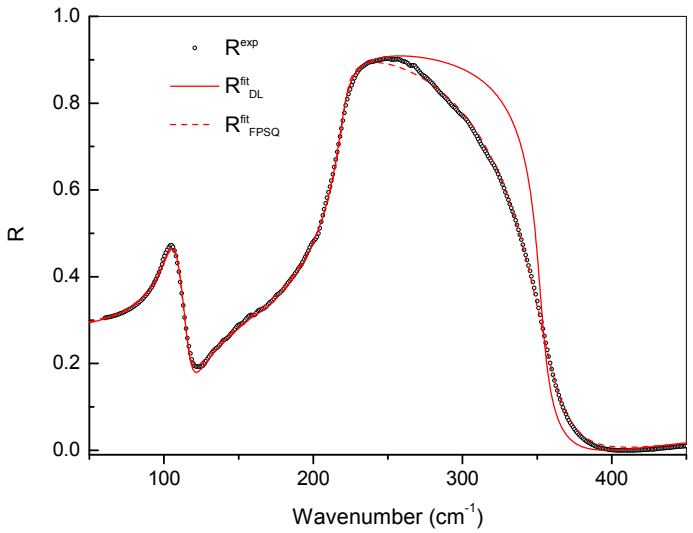

FIG. 3. Zoom over the 150-450 cm^{-1} range of the IR reflectance spectrum along the b axis (B_{2u} symmetry) of aragonite: experimental data (points) versus fitted curves. The fitting is performed based on either the three-parameter Drude-Lorentz model (solid curve) or the Four-Parameter Semi-Quantum model (dashed curve). In both cases the quantum-mechanically computed frequencies and oscillator strengths are taken as initial values for the fitting parameters.

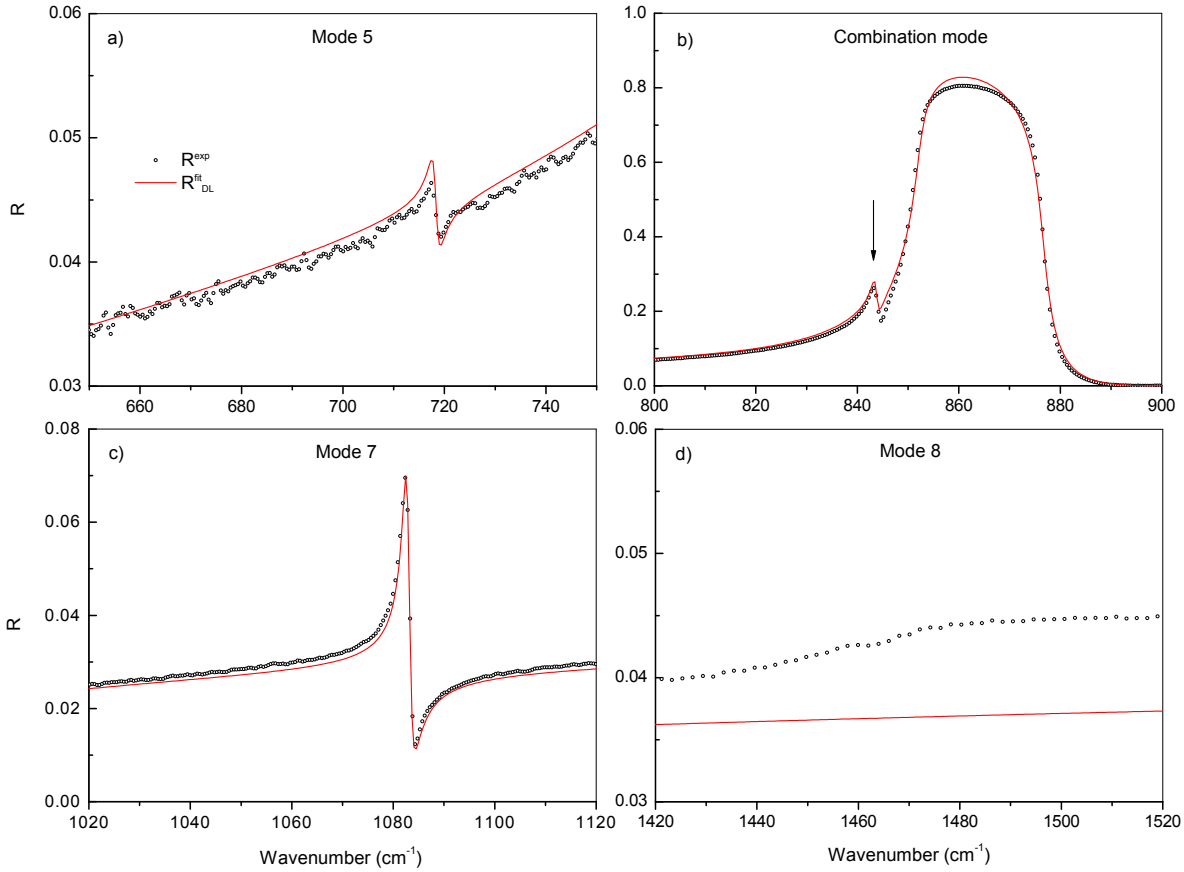

FIG. 4. Zoom over four low intensity features of the IR reflectance spectrum along the a axis (B_{3u} symmetry) of aragonite: experimental data (points) versus fitted curve (solid line). a) mode 5; b) combination mode at 843.6 cm^{-1}; c) mode 7; d) mode 8. See caption to Figure 2 for details on the fitting. Note the very expanded R scale (compare to Figures 2 and 3).

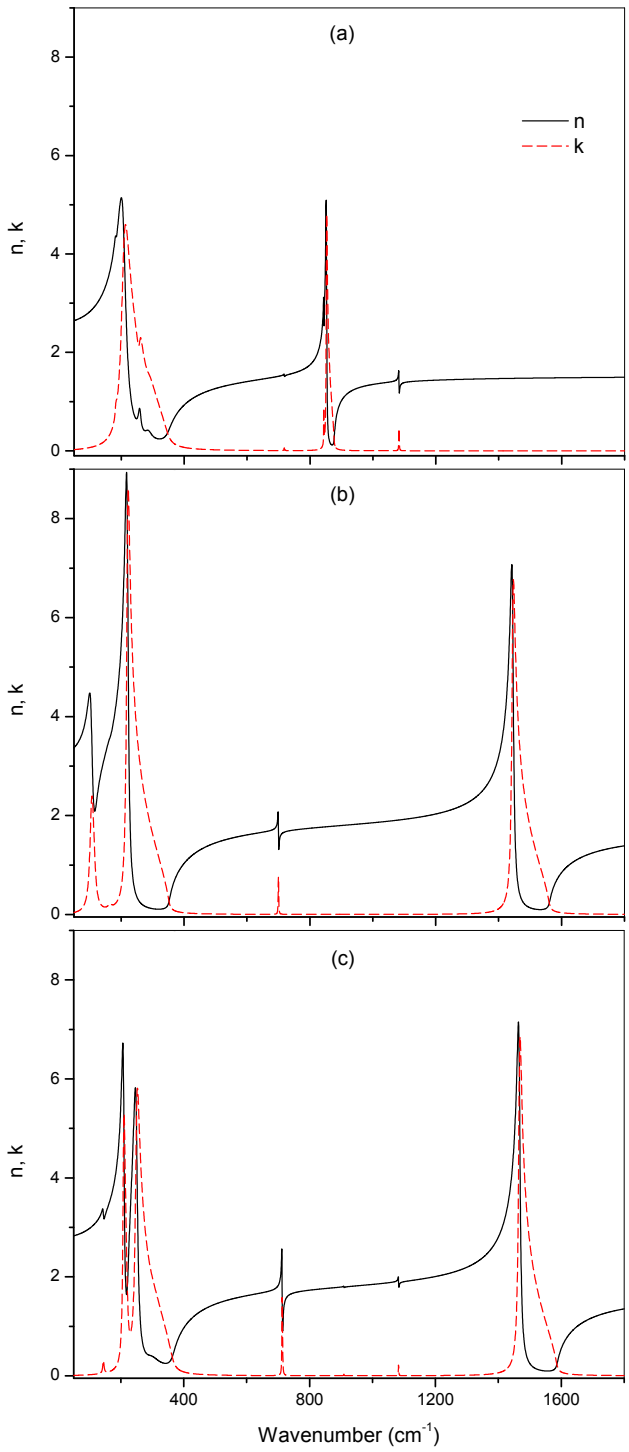

FIG. 5. Refractive (n) and absorption (k) indices along a, b and c axes of aragonite. The two curves are derived from the complex dielectric function ϵ as obtained from best fit with the three-parameter Drude-Lorentz model.

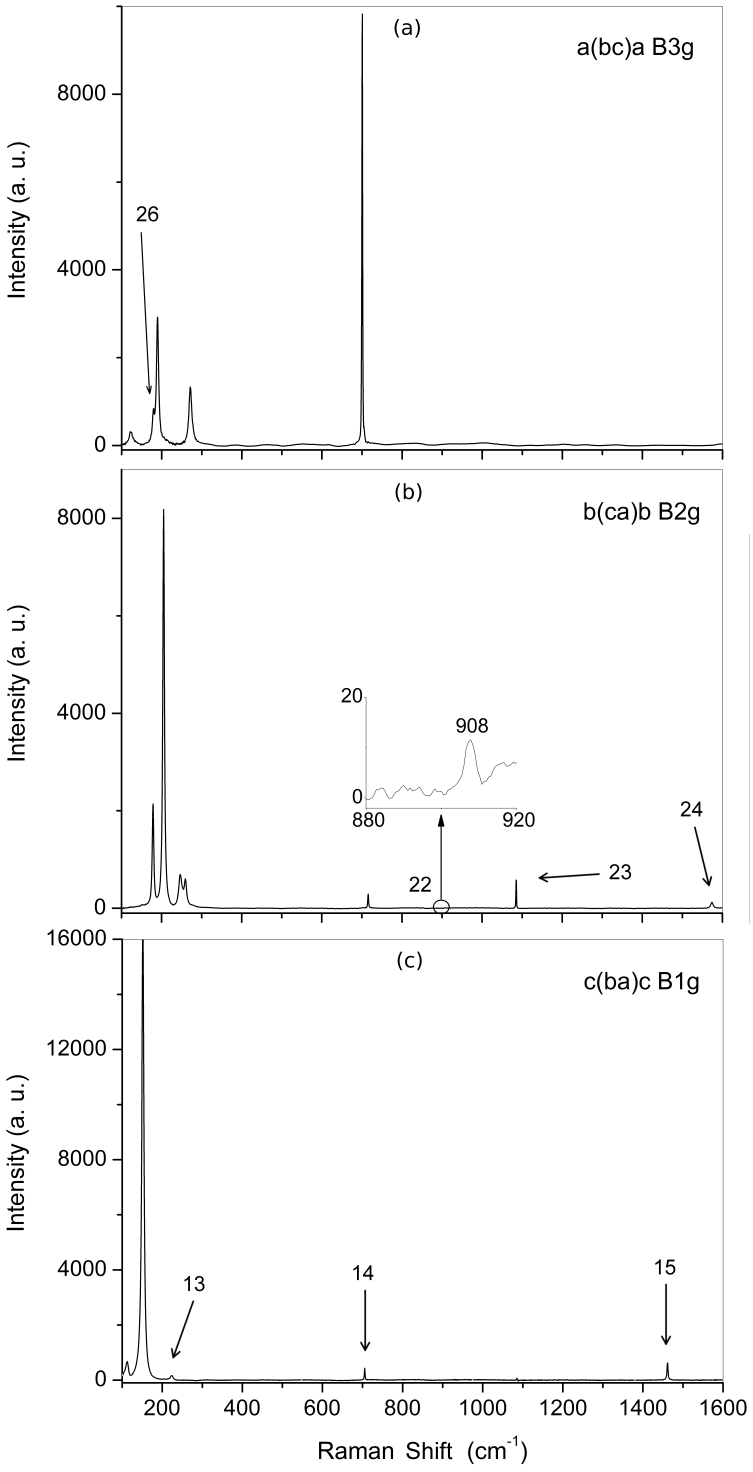

FIG. 6. Experimental polarized Raman spectra for the B_{3g} (a axis), B_{2g} (b axis) and B_{1g} (c axis) symmetries of aragonite. Arrows indicate spectral features discussed in Section IV E (mode labels as in Table VIII).

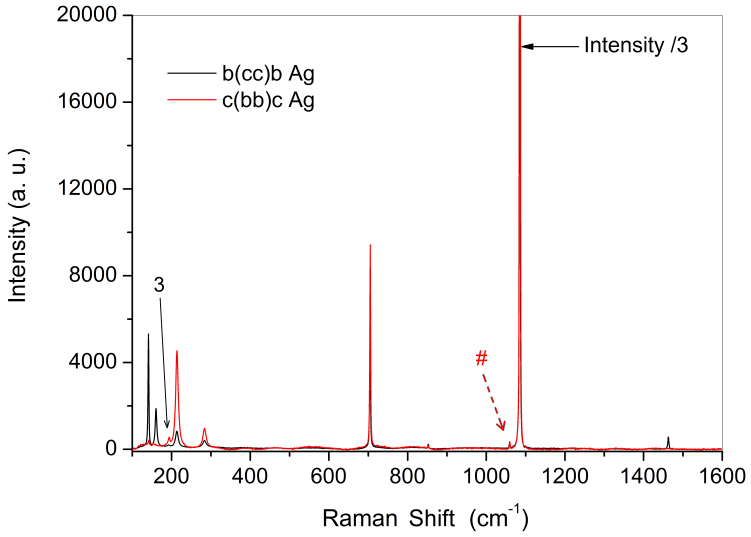

FIG. 7. Experimental polarized Raman spectra for the A_g symmetry of aragonite along the b and c axes. Arrows indicate spectral features discussed in Section IV E (mode labels as in Table VIII). The symbol # marks a ^{18}O isotope mode.

TABLES

	Calc.	Exp.	
		This work	Caspi *et al.* (2005)[13]
a	5.008	4.9633	4.96183
b	8.029	7.9703	7.96914
c	5.861	5.7441	5.74285
V	235.6	227.23	227.081
Ca_x	-0.24031	-0.24044	-0.24015
Ca_z	0.41553	0.41505	0.41502
C_x	-0.08144	-0.08520	-0.0823
C_z	-0.23778	-0.23801	-0.2381
$O1_x$	-0.09008	-0.09530	-0.09453
$O1_z$	-0.07862	-0.07777	-0.07762
$O2_x$	-0.08435	-0.08690	-0.08725
$O2_y$	0.47219	0.47410	0.47499
$O2_z$	-0.31882	-0.31957	-0.31987
d_{C-O1}	1.2789	1.2792	1.2808
d_{C-O2}	1.2891	1.2883	1.2929
d_{Ca-O}	2.4324	2.4162	2.4127

TABLE I. Calculated (B3LYP) and experimental geometry of aragonite (*Pnma* space group, 20 atoms in the unit cell, 4 of which symmetry independent). a, b and c are the cell parameters [Å], V the volume [Å^3]. Atomic coordinates are in fractional units, distances d_{x-y} in Å.

Symm.	IR activity	Raman activity	Optical Modes		
			External	Internal	Total
A_g		α_{xx}, α_{yy}, α_{zz}	5	4	9
B_{1g}		α_{xy}	4	2	6
B_{2g}		α_{xz}	5	4	9
B_{3g}		α_{yz}	4	2	6
A_u			4	2	6
B_{1u}	E $\parallel c$		4	4	8
B_{2u}	E $\parallel b$		3	2	5
B_{3u}	E $\parallel a$		4	4	8

TABLE II. Classification of the vibrational modes of aragonite. Symmetry is obtained from group theory analysis. IR and Raman polarization directions are indicated. External (lattice) and CO_3^{--} internal modes are characterized by very different frequencies, and are easily identified through graphical animation of the eigenvectors.

		TO						LO			TO-LO		
		ν_{calc}	ν_{exp}	$\Delta\nu$	f_{calc}	f_{exp}	Δf	ν_{calc}	ν_{exp}	$\Delta\nu$	$\delta\nu_{calc}$	$\delta\nu_{exp}$	$\Delta\delta$
a (B_{3u})	1	174.1	183.1	-9.0	91.8	60.4	31.40	174.6	183.3	-8.7	0.5	0.2	0.3
	2	210.1	207.8	2.3	3920.2	4105.6	-185.36	353.8	348.4	5.4	143.7	140.6	3.1
	3	269.1	259.2	9.9	62.4	77.4	-15.01	266.9	257.2	9.7	-2.2	-2.0	-0.2
	4	288.9	286.9	2.0	35.0	43.5	-8.53	287.0	284.6	2.4	-1.9	-2.3	0.4
	5	719.2	718.3	0.9	0.1	0.4	-0.26	719.2	718.4	0.8	0.0	0.1	-0.1
	#	–	843.6	–	–	6.1	–	–	–	–	–	–	–
	6	861.9	852.2	9.7	113.1	116.1	-2.98	886.7	876.7	10.0	24.8	24.5	0.3
	7	1092.9	1082.8	10.1	2.4	1.9	0.46	1093.6	1083.3	10.3	0.7	0.5	0.2
	8	1469.9	–	–	0.0	–	–	1469.9	–	–	0.0	–	–
	F [ΔF]				4225.0	4405.3	[244.0]						
b (B_{2u})	1	65.4	105.4	-40.0	6554.9	2228.3	4326.63	83.7	116.5	-32.8	18.2	11.1	7.1
	2	158.7	164.2	-5.5	62.1	53.4	8.66	158.9	164.2	-5.3	0.3	0.0	0.3
	3	198.0	219.9	-21.9	5838.5	4862.0	976.45	343.8	352.5	-8.7	145.8	132.6	13.2
	4	697.4	699.8	-2.4	5.2	6.7	-1.53	698.1	699.0	-0.9	0.7	-0.8	1.5
	5	1445.1	1444.5	0.6	467.1	458.0	9.08	1571.8	1561.0	10.8	126.7	116.5	10.2
	F [ΔF]				12927.7	7608.4	[5322.4]						
c (B_{1u})	1	147.3	144.4	2.9	16.2	59.3	-43.10	147.4	144.9	2.5	0.1	0.5	-0.4
	2	200.7	208.6	-7.9	2617.5	1829.6	787.87	218.4	221.3	-2.9	17.8	12.7	5.1
	3	245.5	249.5	-4.0	2286.7	2423.0	-136.31	359.7	364.2	-4.5	114.2	114.7	-0.5
	4	293.1	298.0	-4.9	7.0	164.9	-157.91	292.8	292.8	0.0	-0.2	-5.2	5.0
	5	712.2	712.4	-0.2	15.5	16.6	-1.12	714.2	714.4	-0.2	2.0	2.0	0.0
	6	913.1	908.8	4.3	0.1	0.2	-0.06	913.1	908.8	4.3	0.0	0.0	0.0
	7	1092.9	1082.8	10.1	1.3	1.1	0.21	1093.1	1082.9	10.2	0.2	0.1	0.1
	8	1474.1	1466.6	7.5	469.2	461.2	8.02	1602.9	1586.0	16.9	128.8	119.4	9.4
	F [ΔF]				5413.5	4955.9	[1134.6]						

TABLE III. Calculated (B3LYP) and experimental (fitted) IR active vibrational frequencies ν [cm^{-1}] and oscillator strengths f (adimensional and multiplied by 10^3) along the a, b and c axes (B_{3u}, B_{2u} and B_{1u} symmetry, respectively) of aragonite. Calculations were performed at the optimized cell volume. Experimental values were obtained through a best fit with the three-parameter Drude-Lorentz model. $\delta\nu$ is the TO-LO splitting. $\Delta\nu$, Δf and $\Delta\delta$ are the differences between calculated and experimental quantities. $F = \sum_n f_n$ is the sum of the oscillator strengths, $\Delta F = \sum_n |\Delta f_n|$ is the sum of the absolute differences between experimental and calculated oscillator strengths. Statistics are reported in Table V. The symbol # indicates a combination mode.

	TO						LO						
	ν_{exp}^{FPSQ}	ν_{exp}^{DL}	$\Delta\nu$	f_{exp}^{FPSQ}	f_{exp}^{DL}	Δf	ν_{exp}^{FPSQ}	ν_{exp}^{DL}	$\Delta\nu$	$\gamma_{TO,exp}^{FPSQ}$	$\gamma_{LO,exp}^{FPSQ}$	$\Delta\gamma_{exp}^{FPSQ}$	γ_{exp}^{DL}
1	105.2	105.4	-0.2	2467.8	2228.3	239.5	116.1	116.5	-0.4	12.5	14.3	-1.8	13.5
2	164.2	164.2	0.0	87.6	53.4	34.2	164.7	164.2	0.5	15.8	15.9	-0.1	15.8
3	221.0	219.9	1.1	5651.8	4862.0	789.8	369.9	352.5	17.4	7.3	35.4	-28.1	9.0
4	699.8	699.8	0.0	7.2	6.7	0.5	700.7	699.0	1.7	1.7	1.8	-0.1	1.7
5	1444.4	1444.5	-0.1	510.2	458.0	52.2	1575.3	1561.0	14.3	9.7	10.4	-0.7	9.0
F [ΔF]				8724.6	7608.4	[1116.2]							
$\overline{\lvert\Delta\rvert}$			0.3			223.2			6.9				
$\overline{\Delta}$			0.2			223.2			6.7				
$\lvert\Delta\rvert_{max}$			1.1			789.8			17.4				

TABLE IV. Difference between IR active experimental frequencies [cm^{-1}], oscillator strengths (adimensional, multiplied by 10^3) and damping factors [cm^{-1}] along the b axis (B_{2u} symmetry) obtained by fitting with the Four-Parameter Semi-Quantum (FPSQ) and the three-parameter Drude-Lorentz (DL) models. $\Delta\nu$ and Δf are the differences between quantities fitted with the two models. $\Delta\gamma_{exp}^{FPSQ}$ is the difference between γ_{TO} and γ_{LO} obtained with the FPSQ model. For F and ΔF see caption to Table III; for statistical indices see caption to Table V.

		ν_{TO}	f	ν_{LO}
a	$\overline{\lvert\Delta\rvert}$	6.3	34.9	6.8
	$\overline{\Delta}$	3.7	-25.8	4.3
	$\lvert\Delta\rvert_{max}$	10.1	185.4	10.3
b	$\overline{\lvert\Delta\rvert}$	14.1	1064.5	11.7
	$\overline{\Delta}$	-13.8	1063.9	-7.4
	$\lvert\Delta\rvert_{max}$	40.0	4326.6	32.8
c	$\overline{\lvert\Delta\rvert}$	5.2	141.8	5.2
	$\overline{\Delta}$	1.0	57.2	3.3
	$\lvert\Delta\rvert_{max}$	10.1	787.9	16.9
Σ	$\overline{\lvert\Delta\rvert}$	7.8	335.05	7.4
	$\overline{\Delta}$	-1.8	279.83	1.0
	$\lvert\Delta\rvert_{max}$	40.0	4326.63	32.8

TABLE V. Statistics on the calculated and experimental IR active vibrational frequencies ν [cm^{-1}] and oscillator strengths f (adimensional, multiplied by 10^3) along the a, b and c axes (respectively B_{3u}, B_{2u} and B_{1u} symmetry) of aragonite (data in Table III). Calculations were performed at the optimized cell volume. Experimental data were obtained from the three-parameter Drude-Lorentz fitting. Statistical indices (x is either ν or f): $\overline{|\Delta|} = \sum_{i=1}^{N} |\Delta x_i|/N$ is the mean absolute difference, $\overline{\Delta} = \sum_{i=1}^{N} \Delta x_i/N$ is the mean difference, $|\Delta_{max}|$ is the maximum difference, N is the number of available experimental data, on which statistics are performed; N is 7, 5 and 8 for the three axes, respectively.

	TO										LO				
	$\nu_{calc}^{E.V.}$	$\nu_{calc}^{O.V.}$	$\Delta\nu_{calc}^{O.V.}$	ν_{exp}	$\Delta\nu_{exp}$	$f_{calc}^{E.V.}$	$f_{calc}^{O.V.}$	$\Delta f_{calc}^{O.V.}$	f_{exp}	Δf_{exp}	$\nu_{calc}^{E.V.}$	$\nu_{calc}^{O.V.}$	$\Delta\nu_{calc}^{O.V.}$	ν_{exp}	$\Delta\nu_{exp}$
1	93.4	65.4	27.9	105.4	-12.0	3670.2	6554.9	-2884.7	2228.3	1441.9	109.6	83.7	25.9	116.5	-6.9
2	172.0	158.7	13.3	164.2	7.8	12.4	62.1	-49.7	53.4	-41.1	172.0	158.9	13.1	164.2	7.8
3	220.8	198.0	22.8	219.9	0.9	4910.5	5838.5	-927.9	4862.0	48.5	360.0	343.8	16.3	352.5	7.5
4	702.0	697.4	4.6	699.8	2.2	6.5	5.2	1.3	6.7	-0.2	702.8	698.1	4.7	699.0	3.8
5	1459.0	1445.1	13.9	1444.5	14.5	476.2	467.1	9.1	458.0	18.2	1586.9	1571.8	15.1	1561.0	25.9
F [ΔF]						9075.8	12927.7	[3872.7]	7608.4	[1549.9]					
$\overline{\lvert\Delta\rvert}$			16.5		7.5			774.5		310.0			15.0		10.4
$\overline{\Delta}$			16.5		2.7			-770.4		293.5			15.0		7.6
$\lvert\Delta\rvert_{max}$			27.9		14.5			2884.7		1441.9			25.9		25.9

TABLE VI. Comparison of IR active calculated frequencies ν [cm^{-1}] and oscillator strengths f (adimensional, multiplied by 10^3) along the b axis (B_{2u} symmetry) obtained at the experimental (E.V.) and optimized (O.V.) lattice parameters. $\Delta\nu_{calc}^{O.V.}$ ($\Delta f_{calc}^{O.V.}$) is the difference between the frequencies (oscillator strengths) calculated at the experimental and optimized lattice parameters; $\Delta\nu_{exp}$ (Δf_{exp}) is the difference between the frequencies (oscillator strengths) calculated at the experimental lattice parameters and the experimental values (obtained from the three-parameter Drude-Lorentz fitting). For F and ΔF see caption to Table III; for statistical indices see caption to Table V.

	ϵ_0			ϵ_∞			F		
	Calc.	Exp.	Δ%	Calc.	Exp.	Δ%	Calc.	Exp.	Δ%
xx (a)	6.406	6.74	-5.0	2.181	2.33	-6.4	4.225	4.41	-4.1
yy (b)	15.588	10.41	+49.7	2.660	2.81	-5.3	12.928	7.61	+70.0
zz (c)	8.087	7.78	+3.9	2.674	2.82	-5.2	5.414	4.96	+9.2

TABLE VII. Calculated (B3LYP) and experimental (fitted) static dielectric tensor (ϵ_0) and its components: the electronic (high frequency) (ϵ_∞) and the ionic contributions, the latter evaluated as the sum of the oscillator strengths ($F = \sum_n f_n$). The three Cartesian directions correspond to the crystallographic ones (indicated in parentheses), so that the dielectric tensor turns out to be diagonal. Experimental values were obtained from the three-parameter Drude-Lorentz fitting of the reflectance spectrum.

			This work		Frech 1980[7]		Alía 1997[55]	
	Symm.	ν_{calc}	ν_{exp}	$\Delta\nu$	ν_{exp}	$\Delta\nu$	ν_{exp}	$\Delta\nu$
1	A_g	148.7	141.5	7.2	142	6.7	143.1	5.6
2		161.9	160.5	1.4	161	0.9	163.5	-1.6
3		195.8	193.8	2.0	193	2.8	–	–
4		205.0	213.5	-8.5	214	-9.0	215.6	-10.6
5		280.2	283.5	-3.3	284	-3.8	284.8	-4.6
6		704.2	704.9	-0.7	705	-0.8	705.7	-1.5
7		862.8	853.0	9.8	853	9.8	853	9.8
#		–	1059.8	–	–	–	–	–
8		1095.3	1085.5	9.8	1085	10.3	1085.7	9.6
9		1473.9	1463.0	10.9	1462	11.9	1462	11.9
10	B_{1g}	97.4	112.6	-15.2	112	-14.6	115.4	-18.0
11		152.1	151.7	0.4	152	0.1	153.3	-1.2
12		199.0	–	–	–	–	–	–
13		213.4	213.9	-0.5	–	–	–	–
14		705.5	705.7	-0.2	721	-15.5	–	–
15		1463.9	1461.5	2.4	–	–	–	–
16	B_{2g}	182.5	178.8	3.7	180	2.5	180.6	1.9
17		207.2	205.1	2.1	206	1.2	206.4	0.8
18		249.2	246.8	2.4	248	1.2	248.5	0.7
19		260.7	259.5	1.2	260	0.7	260.4	0.3
20		278.7	–	–	–	–	–	–
21		714.6	715.8	-1.2	717	-2.4	716.5	-1.9
22		911.8	908.0	3.8	907	4.8	–	–
23		1091.6	1085.0	6.6	–	–	–	–
24		1591.8	1574.0	17.8	1574	17.8	–	–
25	B_{3g}	101.3	122.5	-21.2	123	-21.7	129.3	-28.0
26		167.6	179.6	-12.0	–	–	–	–
27		177.8	189.5	-11.7	190	-12.2	191.3	-13.5
28		271.4	271.5	-0.1	272	-0.6	272.3	-0.9
29		701.2	700.6	0.6	701	0.2	701.3	-0.1
30		1415.0	–	–	–	–	–	–
N				27		23		19
$\overline{\lvert\Delta\rvert}$				5.8		6.6		6.4
$\overline{\Delta}$				0.3		-0.4		-2.2
$\lvert\Delta\rvert_{max}$				21.2		21.7		28.0

TABLE VIII. Calculated (B3LYP, optimized volume) and experimental Raman active vibrational frequencies ν (cm^{-1}) of aragonite. N is the number of experimental data, on which statistical analysis against computed values is performed; statistical indices are defined in the caption to Table V. The symbol # indicates a ^{18}O isotope mode.

[1] W. A. Deer, R. A. Howie, and J. Zussman. *An introduction to the rock-forming minerals.* Longman Group, England, 1992.

[2] P. G. Klepetsanis, P. Drakia, and P. G. Koutsoukos. *Mineral Scale Formation and Inhibition*, pages 251–259. Z. Amjad, Plenum Press, New York and London, 1994.

[3] J. G. Speight. *The Chemistry and Technology of Coal.* CRC Press Inc, 2012.

[4] F. C. Meldrum. Calcium carbonate in biomineralisation and biomimetic chemistry. *Int. Mater. Rev.*, 48:187–224, 2003.

[5] J. W. Morse and F. T. Mackenzie. *Geochemistry of sedimentary carbonates.* Elsevier Science Publishers, 1990.

[6] L. Couture. Vibrational spectra of single ionic crystals. *Ann. Physique*, 2:5–94, 1947.

[7] R. Frech, E. C. Wang, and J. B. Bates. The i.r. and Raman spectra of $CaCO_3$ (aragonite). *Spectrochim. Acta*, 36A:915–919, 1980.

[8] A. Dandeu, B. Humbert, C. Carteret, H. Muhr, E. Plasari, and J.-M. Bossoutrot. Raman spectroscopy - A powerful tool for the quantitative determination of the composition of polymorph mixtures: Application to CaCO3 polymorph mixtures. *Chem. Eng. Technol.*, 29:221–225, 2006.

[9] C. Carteret, A. Dandeu, S. Moussaoui, H. Muhr, B. Humbert, and E. Plasari. Polymorphism studied by Lattice Phonon Raman spectroscopy and Statistical Mixture Analysis Method. Apllication to Calcium Carbonate Polymorphs during Batch Crystallization. *Cryst. Growth Des.*, 9:807–812, 2009.

[10] N. V. Vagenas, A. Gatsouli, and C. G. Kontoyannis. Quantitative analysis of synthetic calcium carbonate polymorphs using FT-IR spectroscopy. *Talanta*, 59:831–836, 2003.

[11] S. R. Dickinson and K. M. McGrath. Quantitative determination of binary and tertiary calcium carbonate mixtures using powder X-ray diffraction. *Analyst*, 126:1118–1121, 2001.

[12] C. G. Kontoyannis and N. V. Vagenas. Calcium carbonate phase analysis using XRD and FT-Raman spectroscopy. *Analyst*, 125:251–255, 2000.

[13] E.N. Caspi, B. Pokroy, P.L. Lee, J.P. Quintana, and E. Zolotoyabko. On the structure of aragonite. *Acta Cryst B*, 61:129–132, 2005.

[14] C.C. Homes, J.M. Tranquada, and D.J. Buttrey. Stripe order and vibrational properties of $La_2NiO_{4+\delta}$ for δ=2/15: Measurements and *ab initio* calculations. *Phys. Rev. B*, 75:045128, 2007.

[15] B. Wyncke, F. Brehat, and H. Kharoubi. Calculation of the reflectivity spectra dependence on the angle of incidence in anisotropic absorbing crystals, application to sodium-nitrite. *Journal of Physics: Condensed Matters*, 2:8791–8800, 1990.

[16] J.C. Decius and R.M. Hexter. *Molecular vibrations in crystals*. McGraw-Hill, 1977.

[17] D. W. Berreman and F. C. Unterwald. Adjusting Poles and Zeros of Dielectric Dispersion to Fit Reststrahlen of $PrCl_3$ and $LaCl_3$. *Phys. Rev.*, 174:791–799, 1968.

[18] F. Gervais and B. Piriou. Anharmonicity in several-polar-mode crystals: adjusting phonon self-energy of LO and TO modes in Al_2O_3 and TiO_2 to fit infrared reflectivity. *J. Phys. C: Solid State Phys.*, 7:2374–2386, 1974.

[19] F. Gervais and B. Piriou. Temperature dependence of transverse- and longitudinal-optic modes in TiO_2 (rutile). *Phys. Rev. B*, 10:1642–1654, 1974.

[20] Alexey Kuzmenko. RefFIT, a software to fit optical spectra. `http://optics.unige.ch/alexey/ reffit.html`.

[21] T.C. Damen, S.P.S. Porto, and B. Tell. Raman effect in Zinc Oxide. *Phys. Rev.*, 142:570–574, 1966.

[22] R. Dovesi, V. R. Saunders, C. Roetti, R. Orlando, C. M. Zicovich-Wilson, F. Pascale, B. Civalleri, K. Doll, N. M. Harrison, I. J. Bush, Ph. D'Arco, and M. Llunell. *CRYSTAL 2009 User's Manual*. University of Torino, Torino, 2009.

[23] R. Dovesi, R. Orlando, B. Civalleri, C. Roetti, V. R. Saunders, and C. M. Zicovich-Wilson. CRYSTAL: a computational tool for the ab initio study of the electronic properties of crystals. *Z. Kristallogr.*, 220:571–573, 2005.

[24] C. M. Zicovich-Wilson, F. Pascale, C. Roetti, V. R. Saunders R. Orlando, and R. Dovesi. The calculation of the vibration frequencies of α-quartz: the effect of Hamiltonian and basis set. *J. Comput. Chem.*, 25:1873–1881, 2004.

[25] M. Prencipe, F. Pascale, C. M. Zicovich-Wilson, V. R. Saunders, R. Orlando, and R. Dovesi. The vibrational spectrum of calcite ($CaCO_3$): an ab initio quantum mechanical calculation. *Phys. Chem. Miner.*, 31:559–564, 2004.

[26] R. Orlando, F. J. Torres, F. Pascale, P. Ugliengo, C. M. Zicovich-Wilson, and R. Dovesi. Vibrational Spectrum of Katoite $Ca_3Al_2[(OH)_4]_3$: A Periodic ab Initio Study. *J. Phys. Chem. B*, 110:692–701, 2006.

[27] R. Dovesi, M. De La Pierre, A. M. Ferrari, F. Pascale, L. Maschio, and C. M. Zicovich-Wilson. The IR vibrational properties of six members of the garnet family: a quantum mechanical ab initio study. *Am. Mineral.*, 96:1787–1798, 2011.

[28] R. Demichelis, H. Suto, Y. Noël, H. Sogawa, T. Naoi, C. Koike, H. Chihara, N. Shimobayashi, M. Ferrabone, and R. Dovesi. The infrared spectrum of ortho-enstatite from reflectance experiments and first-principle simulations. *Mon. Not. R. Astron. Soc.*, 420:147–154, 2012.

[29] Y. Noël, M. De La Pierre, L. Maschio, M. Rérat, C. M. Zicovich-Wilson, and R. Dovesi. Electronic Structure, Dielectric Properties and Infrared Vibrational Spectrum of Fayalite: An Ab Initio Simulation With an All-Electron Gaussian Basis Set and the B3LYP Functional. *Int. J. Quantum Chem.*, 112:2098–2108, 2012.

[30] A. D. Becke. Density-Functional Thermochemistry 3. The Role of Exact Echange. *J. Chem. Phys.*, 98:5648–5652, 1993.

[31] W. Koch and M. C. Holthausen. *A Chemist's Guide to Density Functional Theory.* Wiley-VCH Verlag GmbH, Weinheim, 2000.

[32] F. Pascale, C. M. Zicovich-Wilson, R. Orlando, C. Roetti, P. Ugliengo, and R. Dovesi. Vibration frequencies of $Mg_3Al_2Si_3O_{12}$ pyrope. An *ab initio* study with the CRYSTAL code. *J. Phys. Chem. B*, 109:6146–6152, 2005.

[33] F. Pascale, M. Catti, A. Damin, R. Orlando, V. R. Saunders, and R. Dovesi. Vibration frequencies of $Ca_3Fe_2Si_3O_{12}$ andradite. An *ab initio* study with the CRYSTAL code. *J. Phys. Chem. B*, 109:18522–18527, 2005.

[34] C.M. Zicovich-Wilson, M.L. San-Roman, M.A. Camblor, F. Pascale, and S. Durand-Niconoff. Structure, vibrational analysis, and insights into host-guest interactions in as-synthesized pure silica ITQ-12 zeolite by periodic B3LYP calculations. *J. Am. Chem. Soc.*, 129:11512–11523, 2007.

[35] C. M. Zicovich-Wilson, J. Torres, F. Pascale, L. Valenzano, R. Orlando, and R. Dovesi. The *ab initio* simulation of the IR spectra of Pyrope, Grossular and Andradite. *J. Comput. Chem.*, 29:2268–2278, 2008.

[36] L. Valenzano, F. J. Torres, K. Doll, F. Pascale, C. M. Zicovich-Wilson, and R. Dovesi. Ab Initio Study of the Vibrational Spectrum and Related Properties of Crystalline Compounds; the Case of $CaCO_3$ Calcite. *Z. Phys. Chem.*, 220:893–912, 2006.

[37] F. Pascale, C. M. Zicovich-Wilson, F. Liópez Gejo, B. Civalleri, R. Orlando, and R. Dovesi. The calculation of the vibrational frequencies of crystalline compounds and its implementation in the CRYSTAL code. *J. Comput. Chem.*, 25:888–897, 2004.

[38] G. M. Barrow. *Introduction to molecular spectroscopy.* McGraw-Hill, New York, 1962.

[39] B. A. Hess, L. J. Schaad, P. Carsky, and R. Zahradnik. Ab Initio Calculations of Vibrational Spectra and Their Use in the Identification of Unusual Molecules. *Chem. Rev.*, 86:709–730, 1986.

[40] S. Dall'Olio, R. Dovesi, and R. Resta. Spontaneous polarization as a Berry phase of the Hartree-Fock wave function: The case of $KNbO_3$. *Phys. Rev. B*, 56:10105–10114, 1997.

[41] P. Baranek, C. M. Zicovich-Wilson, C. Roetti, R. Orlando, and R. Dovesi. Well-localized crystalline orbitals obtained from Bloch functions: the case of $KNbO_3$. *Phys. Rev. B*, 64:125102, 2001.

[42] Y. Noel, C. Zicovich-Wilson, B. Civalleri, Ph. D'arco, and R. Dovesi. Polarization properties of ZnO and BeO: an ab initio study through the Berry phase and Wannier functions approaches. *Phys. Rev. B*, 65:014111, 2002.

[43] M. Ferrero, M. Rérat, R. Orlando, and R. Dovesi. The calculation of static polarizabilities of periodic compounds. The implementation in the CRYSTAL code for 1D, 2D and 3D systems. *J. Comput. Chem.*, 29:1450–1459, 2008.

[44] M. Ferrero, M. Rérat, R. Orlando, and R. Dovesi. Coupled perturbed Hartree-Fock for periodic systems: the role of symmetry and related computational aspects. *J. Chem. Phys.*, 128:014110, 2008.

[45] M. Ferrero, M. Rérat, B. Kirtman, and R. Dovesi. Calculation of first and second static hyperpolarizabilities of one- to three-dimensional periodic compounds. Implementation in the CRYSTAL code. *J. Chem. Phys.*, 129:244110, 2008.

[46] M. Ferrero, M. Rérat, R. Orlando, and R. Dovesi. *Coupled Perturbed Hartree-Fock Calculation of the static polarizability for periodic systems: implementation in the CRYSTAL code*, volume Computation in Modern Science and Engineering, Volume 2B of *AIP Conference Proceedings.* T. E. Simos and G. Maroulis, American Institute of Physics, 2007.

[47] M. Ferrero, B. Civalleri, M. Rérat, R. Orlando, and R. Dovesi. The calculation of the static first and second susceptibilities of crystalline urea: a comparison of Hartree-Fock and density functional theory results obtained with the periodic coupled perturbed Hartree-Fock/Kohn-Sham scheme. *J. Chem. Phys.*, 131:214704, 2009.

[48] P. Ugliengo, D. Viterbo, and G. Chiari. Moldraw utility. `http://www.moldraw.unito.it`.

[49] P. Ugliengo, D. Viterbo, and G. Chiari. Moldraw: Molecular graphics on a personal computer. *Z. Kristallogr.*, 207:9–23, 1993.

[50] Jmol program.
`http://jmol.sourceforge.net/`.

[51] Inkscape program.
`http://www.inkscape.org/`.

[52] Libreoffice suite.
`http://www.libreoffice.org/`.

[53] W. B. White. The Carbonate Minerals. In *The Infrared Spectra of Minerals*, pages 227–284. V. C. Farmer, Mineralogical Society of America, 1974.

[54] M. Donoghue, P. H. Hepburn, and S. D. Ross. Factors affecting the infrared spectra of planar anions with D_{3h}, symmetry V: The origin of the splitting of the out-of-plane bending mode in carbonates and nitrates. *Spectrochim. Acta A*, 27:1065–1072, 1971.

[55] J. M. Alía, Y. Díaz de Mera, H. G. M. Edwards, P. González Martín, and S. López Andrés. FT-Raman and infrared spectroscopic study of aragonite-strontianite ($Ca_xSr_{1x}CO_3$) solid solution. *Spectrochim. Acta A*, 53:2347–2362, 1997.